Medical diagnostic systems

(Orvosbiológiai képalkotó rendszerek)

Modelling ultrasound image formation

(Ultrahang képalkotás modellezése)

Miklós Gyöngy

TÁMOP – 4.1.2-08/2/A/KMR-2009-0006

Quick reminder #1: linear time-invariant systems

Suppose

- System $w(t) \rightarrow a(t)$ is linear time-invariant
  - $\alpha w_1(t) + \beta w_2(t) \rightarrow \alpha a_1(t) + \beta a_2(t)$
  - $w(t-\tau) \rightarrow a(t-\tau)$
- $\delta(t) \rightarrow h(t)$ (impulse response)
- Fourier transform $\mathcal{F}\{h(t)\} = H(f)$ (frequency response)

Then

- $a(t) = h(t) *_t w(t) = \int_{\tau:[-\infty,+\infty]} h(\tau) w(t-\tau)\, d\tau$ (temporal convolution)
- $A(f) = H(f) W(f)$

Model ultrasonic image formation as linear time-invariant?

Quick reminder #2: point spread functions

- Point spread function $\mathbf{P}$ is 2-D equivalent of impulse response
- Assuming $\mathbf{P}$ is spatially invariant, $\mathcal{F}_{2D}\{\mathbf{P}*_{2D}\mathbf{T}\} = \mathcal{F}_{2D}\{\mathbf{P}\}\mathcal{F}_{2D}\{\mathbf{T}\}$
- Typically, $\mathbf{P}$ is Gaussian-type blurring function (or low-pass filter)
- Arises in optics, when structures in original scene are larger than wavelength
- For sub-wavelength structures illuminated by coherent light or ultrasound, interference of scatterered radiation occurs, resulting in speckle

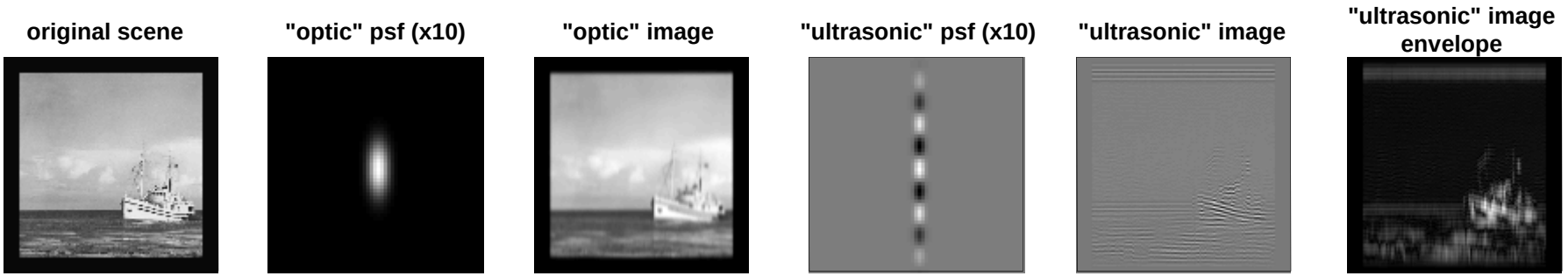

Original photograph in public domain. Credit: Victor B. Scheffer / US Fish and Wildlife Service (www.fws.gov/digitalmedia)

The imaging process

- input waveform temporally filtered by electromechanical response
- beamforming operations temporal filters that act as spatial filters on medium
- above create point spread function (**P**) of imaging system
- assume small region of interest (ROI) where **P** is spatially invariant
- beamformed image **B** convolution of *tissue impulse response* **T** with **P**
- envelope operation not linear (no *psf*) but there is a characteristic beam size
- scattering within beam (resolution cell) leads to interference effects

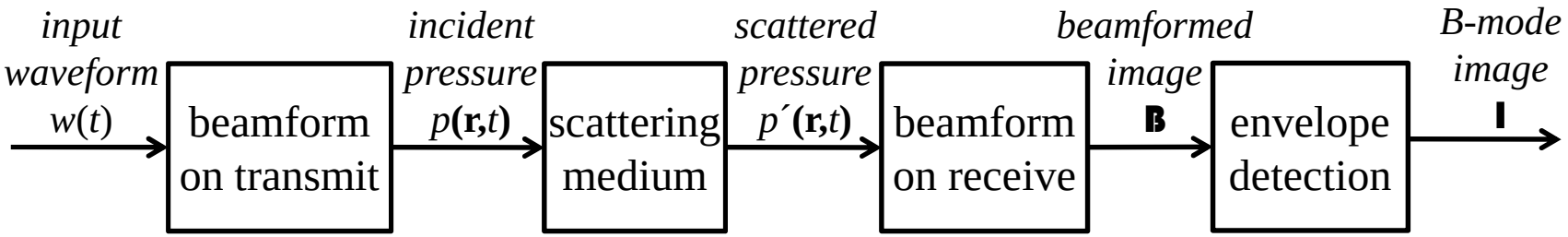

Overview of this lecture

Three approaches to calculating point spread function **P**

1. Point element (**PE**) approximation: array elements as point transceivers
2. Spatial impulse response (**SIR**): convolution of impulse response with input waveform yields actual response
3. Frequency-domain (**FD**) analysis: consider transmit-receive beam shape at carrier frequency of input waveform and multiply by input waveform

Calculating beamformed image **P** * **T** = **B**

- origin of tissue impulse response **T**
- models for **T**
- image speckle – junk or disguised information?

Brief notes on quantitative ultrasound (QUS) and simulation software

Point element (PE) approximation

- N point transceivers with uniform frequency response
- Define $r_{ab} := |\mathbf{r}_b - \mathbf{r}_a|$; $\tau_{ab} := r_{ab}/c$
- Pressure wavefronts focussed to $\mathbf{r}_f$
- Total incident pressure at $\mathbf{r}_a$ sum of point sources at $\mathbf{r}_n$

$$p(\mathbf{r}_a,t)=\sum_n A_n/r_{na}\, w(t-(\tau_{na}-\tau_{0a})+\tau_{nf})$$

  where A_n are *apodization* weights
- Monopolar scatterer at $\mathbf{r}_s$ with scattering strength s_s
- Scattered pressure recorded at $\mathbf{r}_n$

$$p'(\mathbf{r}_n,t) = s_s/r_{sn}\; p(\mathbf{r}_s,\, t - \tau_{sn})$$

- Beamformed image (using two-way travel time)

$$\mathbf{B}(\mathbf{r}_a) = \sum_n A_n\, r_{na}\, p'(\mathbf{r}_n,\, 2\tau_{na})$$

- Sanity check: $\mathbf{r} = \mathbf{r}_{\{0,a,f,s\}}$; $\tau_n = \tau_{\{0,a,f,s\}n}$; $A_n = 1/N$

$$\mathbf{B}(\mathbf{r}) = 1/N^2 \sum_n\sum_n w(2\tau_n - \tau_n - \tau_n + \tau_n - \tau_n) = w(0)$$

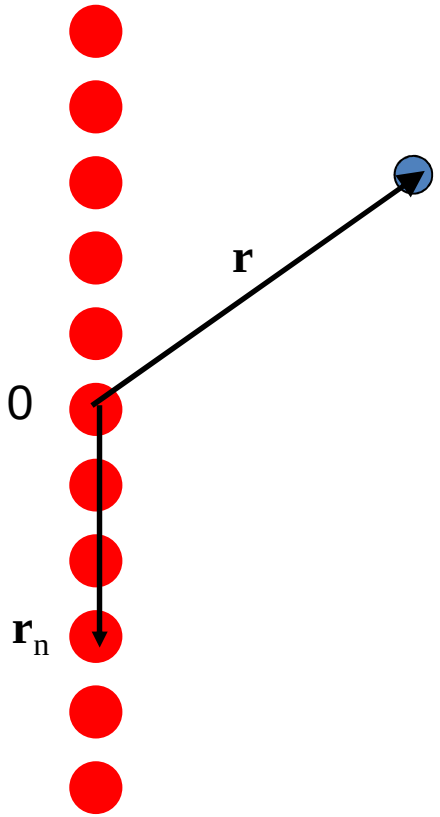

PE approximation: example

$N = 128$; $D = 19$ mm; $c = 1500$ m/s; $f_0 = 7.5$ MHz; $\mathbf{r}_f = (0,0,75$ mm);

$w(t) = \cos(2\pi f_0 t)\ \{\cos(\pi f_0 t/3)\mathrm{rect}(f_0 t/3)\}$ (3 cycles of cosine-modulated 7.5 MHz)

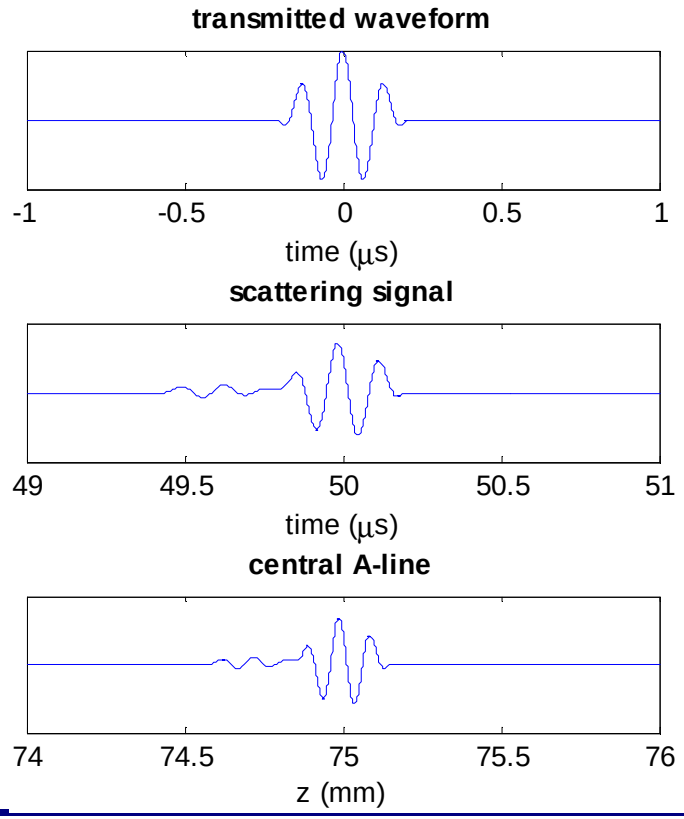

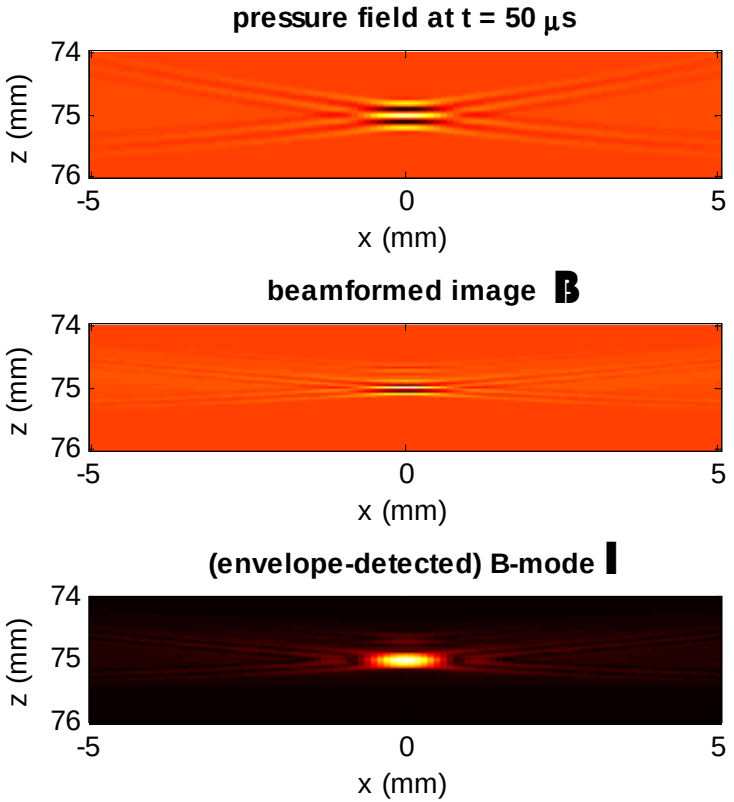

PE approximation: validity (or otherwise)

- Typical array element: $D_{\{x,y\}} = \{0.3\text{ mm}, 5\text{ mm}\}$, $f_0 = 7.5$ MHz
- Far-field distance: $D_{\{x,y\}}^2 f/4c = 0.1\text{ mm}, 31\text{ mm}$ [Olympus 2006]
- In practice, far-field usually brought even closer due to elevational focusing
- By using more elements along elevation direction to model transducer, accuracy is increased, especially of sensitivity along elevational direction
- In limit of $N \to \infty$
  - array becomes continuous surface
  - sum becomes integration
  - expression reflects Huygen's principle
  - analytical solutions sometimes possible

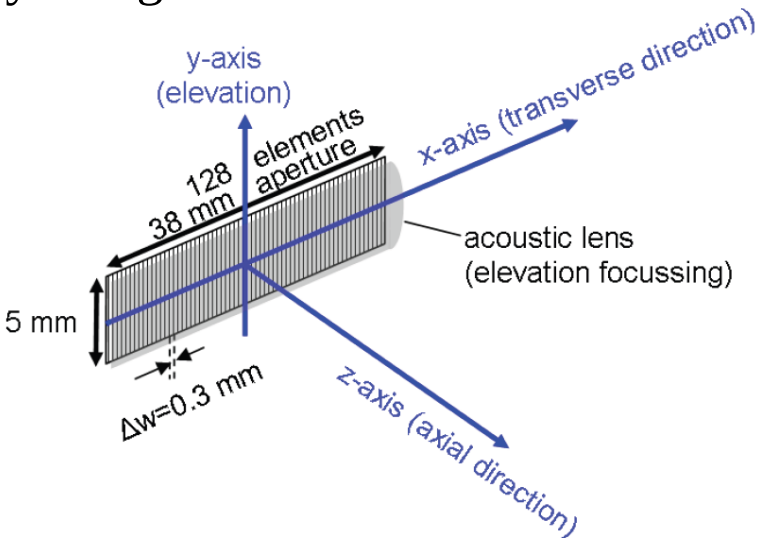

[Gyöngy 2010]

Huygen's principle

- Pressure from integral of contributions across surface
- Let acceleration d$v(\mathbf{r}')/dt$ of surface be $A(\mathbf{r}')w(t)$
- Then, Rayleigh integral [Jensen 1999] becomes

$$p(\mathbf{r},t)=(\rho_0/2\pi)\int A(\mathbf{r}')/|\mathbf{r}-\mathbf{r}'|\; w(t-|\mathbf{r}-\mathbf{r}'|/c-\tau(\mathbf{r}'))\; d\mathbf{r}'$$

- NB: using form of Rayleigh integral without angle-dependent *obliquity factor* [Goodman 1996, p. 51]
- Pressure response $h_1(\mathbf{r},t)$ to $w(t)=\delta(t)$? (SIR)

$$h_1(\mathbf{r},t) = (\rho_0/2\pi)\int A(\mathbf{r}')/|\mathbf{r}-\mathbf{r}'|\; \delta(t-|\mathbf{r}-\mathbf{r}'|/c-\tau(\mathbf{r}'))\; d\mathbf{r}'$$

- Pressure response $H_1(\mathbf{r},f)$ to $w(t)=\exp(j2\pi ft)$? (FD)

$$H_1(\mathbf{r},f) = (\rho_0/2\pi)\int A(\mathbf{r}')/|\mathbf{r}-\mathbf{r}'|\; \exp[j2\pi f(t-|\mathbf{r}-\mathbf{r}'|/c-\tau(\mathbf{r}'))]\; d\mathbf{r}'$$

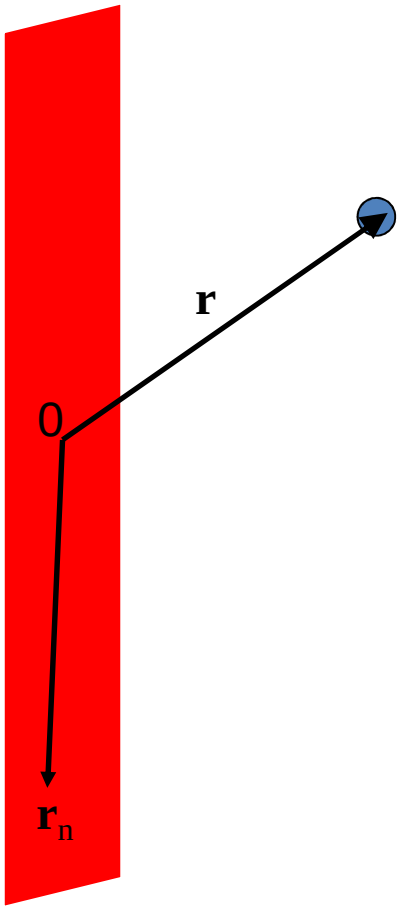

Spatial impulse response (SIR) [Jensen 1999]

- Pressure response $h_1(\mathbf{r},t)$ to $w(t)=\delta(t)$

$$h_1(\mathbf{r},t) = (\rho_0/2\pi)\int A(\mathbf{r'})/|\mathbf{r}-\mathbf{r'}|\ \delta(t-|\mathbf{r}-\mathbf{r'}|/c-\tau(\mathbf{r'}))\ d\mathbf{r'}$$

- Pressure response to arbitrary $w(t)$

$$p(\mathbf{r},t)= h_1(\mathbf{r},t)*_t w(t)$$

- **$h_1(\mathbf{r},t)$ known as SIR: response $p(\mathbf{r},t)$ due to transducer excited by impulse**
- What does spatial impulse response look like? Assume focal point $\mathbf{r}_f$ and time of arrival t_f
  - at point of focal formation: $h_1(\mathbf{r}_f,t)\ \alpha\ \delta(t-t_f)$
  - outside it, response is blurred by imperfect focusing

Next: consider SIR of three transducer shapes (all unfocussed and unapodised)

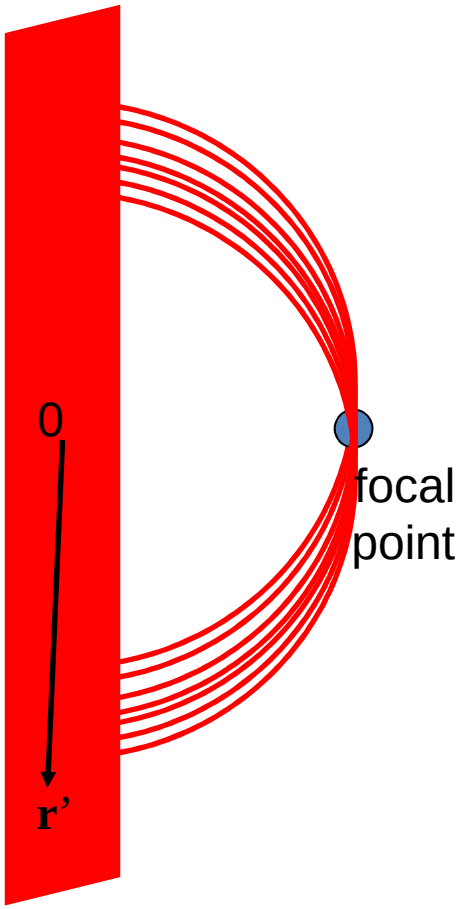

Example 1: Axial SIR of circular transducer

[Cobbold 2007, p. 113]

$$h_1([0,0,z],t) = (\rho_0/2\pi)\int_{|\mathbf{r'}|<a} \delta(t-|[0,0,z]-\mathbf{r'}|/c) \,/|[0,0,z]-\mathbf{r'}|\, d\mathbf{r'}$$

- Cylindrical co-ordinates:

$$h_1([0,0,z],t) = (\rho_0/2\pi)\int_{r':[0,a]} \delta(t-R/c) \,/R\, 2\pi r'\, dr'$$

- Substitution $R^2 = r'^2+z^2$:

$$h_1([0,0,z],t) = \rho_0\int_{R:[z,(a^2+z^2)^{1/2}]} \delta(t-R/c) \,/R\, r'\, dr'$$

$$= \rho_0 c[\,\cancel{H}(t-z/c) - \cancel{H}(t-(a^2+z^2)^{1/2}/c)]$$

- For each R, equal contribution to final waveform!
- Integration of equally-weighted δ yields rect function
- For impulse velocity (rather than acceleration) across surface, two opposing δ are generated: one from centre (*direct wave*) and one from edge (*edge wave*)

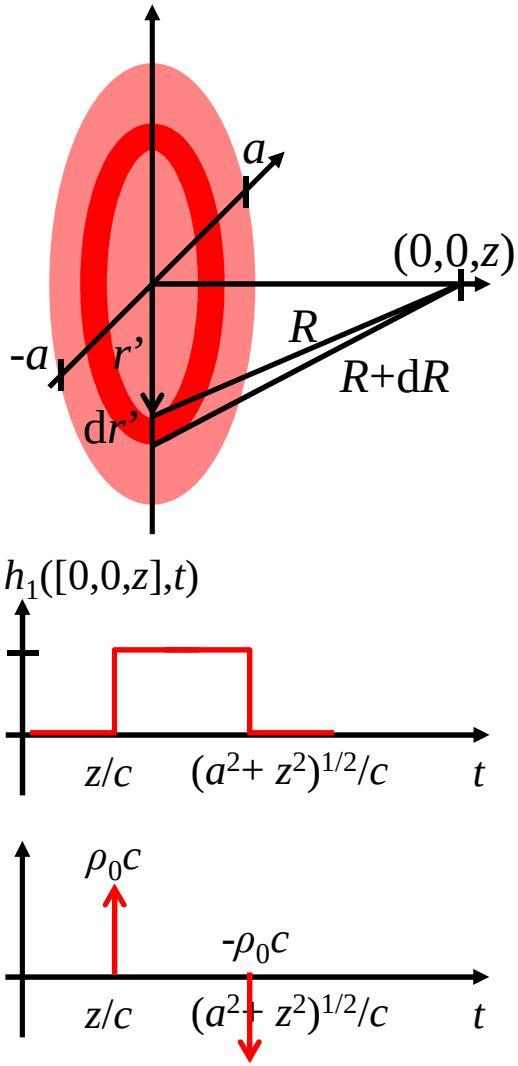

Example 2: Far-field SIR of rectangular transducer [Ellis *et al.* 2007]

- Define propagation time values t_1,t_2,t_3,t_4 from corners of rectangle to **r** (in ascending order)
- Far-field approximations
  1. no wavelet from rectangle can reach **r** until t_1 (0 response)
  2. no wavelet will reach **r** after t_4 (0 response)
  3. maximum and uniform response between t_3 and t_4
  4. linear increase and decrease during intermediate times
- Above approximations lead to a trapezoid response
- Linear arrays consist of rectangular elements (though elevational focusing lens is placed in front of them)
- Arbitrary shapes decomposed into rectangular elements

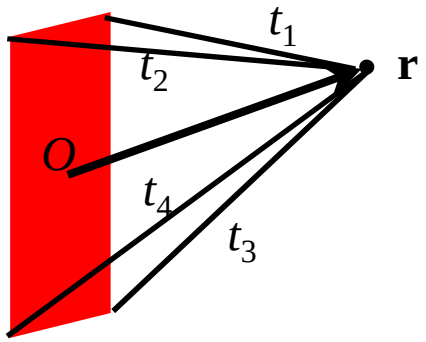

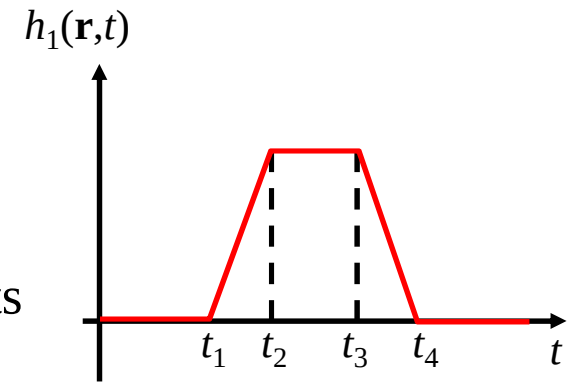

Example 3: Polygon [Jensen 1999]

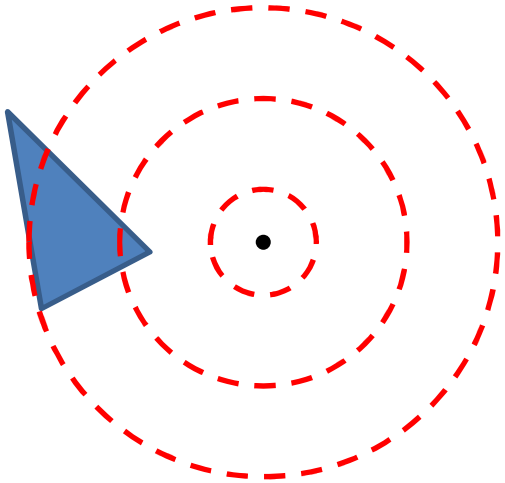

- Acoustic reciprocity: pressure recorded by point receiver *B* due to point source *A* remains the same if locations of source and receiver are interchanged
- More generally, if source consists of sum/integration of point sources over surface *A*, pressure recorded at *B* is equivalent to sum/integration of pressures over *A* caused by point source at *B*
- Intersection of spherically spreading wave with polygon is set of circular arcs whose total length determines magnitude of pressure received
- Validity of acoustic reciprocity: arcs form region of polygon that determines $p(\mathbf{r},t)$
- Arbitrary shapes decomposed into polygons

SIR: calculation of ℘

- Pulse-echo SIR for unity strength point scatterer at **r** is:

$$h_1(\mathbf{r},t) *_t h_1(\mathbf{r},t)$$

- Therefore, *psf* is

$$℘ = w(t) *_t h_1(\mathbf{r},t) *_t h_1(\mathbf{r},t)$$

- Example: a=45 mm; $A(\mathbf{r})$=1; z_s=60 mm; f_0=0.5 MHz; $w(t) = \cos(2\pi f_0 t)\ \{\cos(\pi f_0 t/5)\mathrm{rect}(f_0 t/5)\}$;

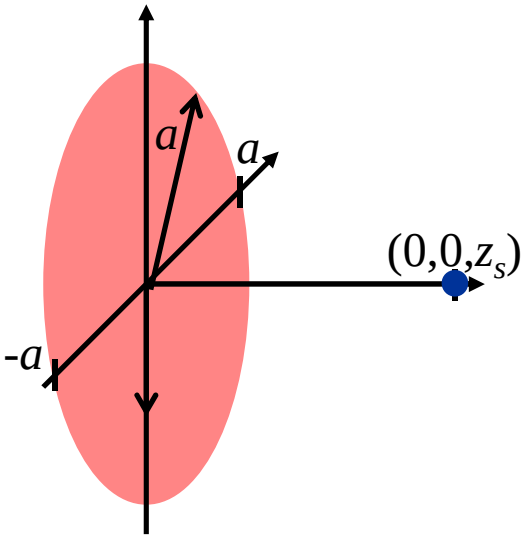

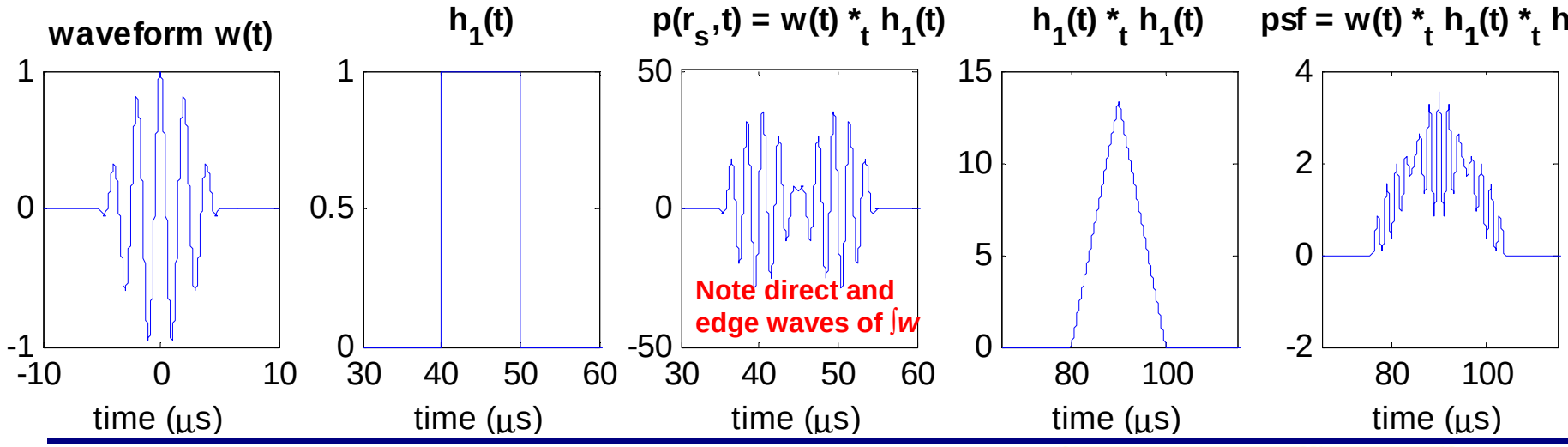

Frequency-domain (FD) method

- Pressure response $H_1(\mathbf{r},f)$ to $w(t)=\exp(j2\pi ft)$

  $H_1(\mathbf{r},f) = (\rho_0/2\pi)\int A(\mathbf{r'})/|\mathbf{r}-\mathbf{r'}| \exp[j2\pi f(t-|\mathbf{r}-\mathbf{r'}|/c-\tau(\mathbf{r'})]\, d\mathbf{r'}$
- Pressure in focal plane is Fourier transform of A(**r'**)!
- Proof:
  - Assume transducer is on *x*-*y* plane
  - Focusing at $t=0$, $\mathbf{r}=(0,0,z_f)$, $\tau(x',y')=-(x'^2+y'^2+z'^2)^{1/2}/c$
  - $x',y' \ll z_f$; approximation $1/|\mathbf{r}-\mathbf{r'}|\approx 1/z_f$
  - $x',y' \ll z_f$; Fresnel approximation $(z_f^2+x'^2+y'^2)^{1/2}\approx z_f+(x'^2+y'^2)/2z_f$
  - $H_1(x,y,z_f) = (\rho_0/2\pi z_f) \iint A(x',y') \exp[j(\omega t-k\varphi)]\, dx'dy'$
  - $\varphi=((x-x')^2+(y-y')^2+z_f)^{1/2} - (x'^2+y'^2+z'^2)^{1/2} \approx (x^2-2xx'+y^2-2yy')/2z_f$
  - $\mathbf{|H_1(x,y,z_f)| = (\rho_0/2\pi z_f) \iint A(x',y') \exp[jk(xx'+yy')]\, dx'\, dy'}$

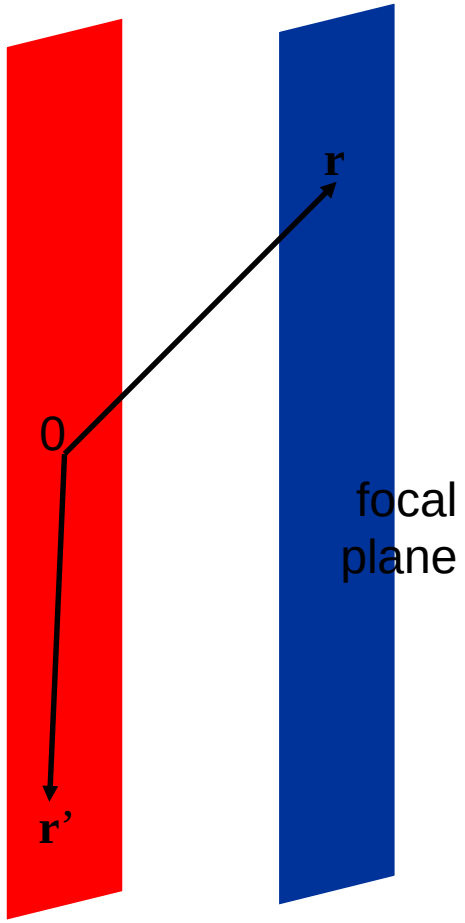

FD method

- Pressure in focal plane is 2-D Fourier transform of A(**r**')!
- Circular aperture: Airy patterns (cf. optical lenses)
- Uniform apodization across rectangular aperture D_x, D_y
  - $|H_1(x,0,z_f)| = (\rho_0/2\pi z_f)\ \mathrm{sinc}(x/f_{\#:x}\lambda)\ \mathrm{sinc}(y/f_{\#:x}\lambda)$
  - $f_{\#:x} = z_f/D_x$; $f_{\#:x} = z_f/D_x$, (f-number in *x* and *y* directions)
  - $\mathrm{sinc}(\pm 0.443) \approx 1/\sqrt{2}$; -3dB beam width (one-way!) is $\approx 0.89 f_{\#}\lambda$
  - Increasing *D*, or decreasing z_f or λ, all narrow the beam
  - Just as in spectrum analysis, windowing function (typically) reduces sidelobes at cost of increasing main lobe width
- Electronic steering of discrete elements
  - Fourier theory: multiplication in space ↔ convolution in frequency
  - If discrete elements modelled as multiplication with dirac deltas (point sources as before), this creates *grating lobes*

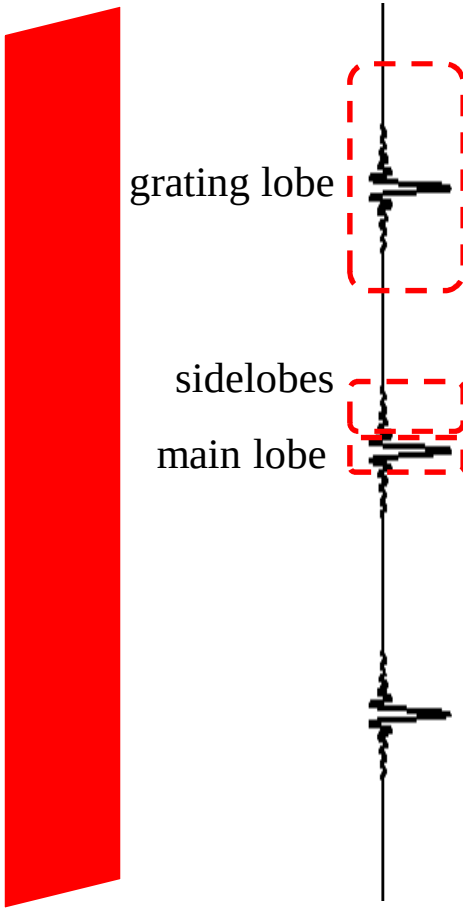

FD: central beam dimensions

- Recap: beam in focal plane 2-D Fourier transform of aperture function $A(x,y)$
- One-way beam in focal plane (x,y,z_f) for uniform aperture:

$$|H_1(x,y,z_f)| = (\rho_0/2\pi z_f)\ \mathrm{sinc}(x/f_{\#:x}\lambda)\ \mathrm{sinc}(y/f_{\#:y}\lambda)$$

- Beam along z-axis? **Fresnel transform of *A*(*x*,*y*)!** [Mast 2007; Gyöngy 2010]
- Fresnel integral:

$$\mathrm{Fr}(z) = \int_{l:[0,z]} \exp(j\pi l^2/2)\ \mathrm{d}l$$

- In analogy with sinc function, define Fresnc function [Gyöngy 2010]:

$$\mathrm{Fc}(z) = \mathrm{Fr}(z_2)/z_2 \text{ where } z_2 = (z/2)^{1/2}$$

- Beam in axial direction is approximated by larger aperture dimension:

$$|H_1(z,z_f)| = \mathrm{Fc}(\Delta z/f_\#^2\lambda); \qquad f_\# = \min(f_{\#:x}, f_{\#:y})$$

FD: Gaussian approximation to central beam

- Reciprocity theorem: transmit and receive beams identical
- One-way (transmit or receive) -3dB beam widths along x, y, z:

$$(\Delta_{x3}, \Delta_{y3}, \Delta_{z3}) = (0.89f_{\#:x}\lambda, 0.89f_{\#:y}\lambda, 6.95f_{\#}^{2}\lambda)$$

- 3-D Gaussian function with -3dB beam widths Δ_{x3}, Δ_{y3}, Δ_{z3}:

$$\exp\{(0.59x/\Delta_{x3})^2 + (0.59y/\Delta_{y3})^2 + (0.59z/\Delta_{z3})^2\}$$

- Thus, beam can be approximated by Gaussian function

$$\exp\{-(0.66x/f_{\#:x}\lambda)^2 - (0.66y/f_{\#:y}\lambda)^2 - (0.085z/f_{\#}^{2}\lambda)^2\}$$

- Two way (transmit-receive)

$$\exp\{-2(0.66x/f_{\#:x}\lambda)^2 - 2(0.66y/f_{\#:y}\lambda)^2 - 2(0.085z/f_{\#}^{2}\lambda)^2\}$$

FD: estimating ρ for pulsed waveform $w(t)$

- Typically $w(t)/c << \Delta_{z3}$
- ρ in axial direction determined by $w(t)$
- ρ in transverse direction determined by CW beam of carrier frequency
- Thus, estimate ρ as product of CW beam by waveform
- Compare result with PE method (simulation parameters identical)

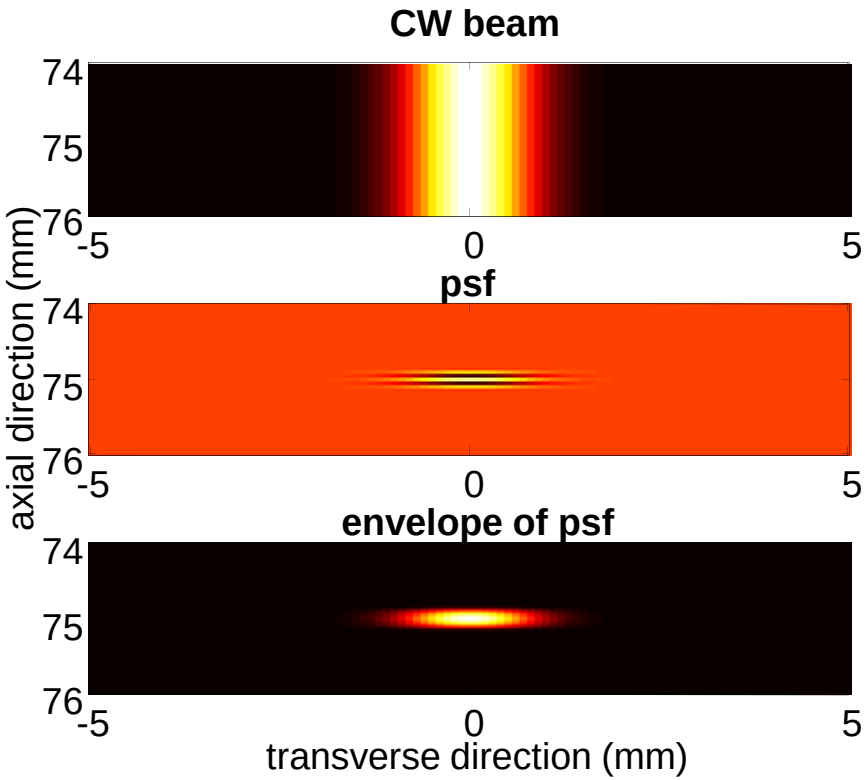

Summary of different approaches to calculating p

Point element (**PE**) approximation

- Arbitrary accuracy achievable
- Simple calculation
- Large number of points may make computation slow

Spatial impulse response (**SIR**)

- Often simple analytical expression exists for SIR
- SIR specific to imaging array only: no recalculation needed if $w(t)$ changed
- Large sampling rate needed to make convolution accurate

Frequency-domain (**FD**) analysis

- Conceptually simple
- Inaccurate extension to pulsed waveform

Calculating beamformed image

- Simple shift-invariant model: beamformed image

$$\mathbf{B}=\mathbf{P} *_{2D} \mathbf{T}$$

- B-mode image obtained by taking envelope of $\mathbf{B}$
- We have found models to estimate $\mathbf{P}$
- Where does tissue impulse response $\mathbf{T}$ come from?
- How do we model it?
- What is image speckle – junk or disguised information?

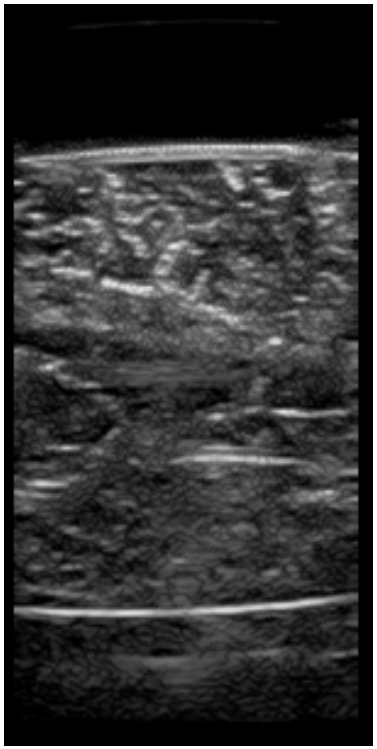

B-mode image of bovine liver sample in water

Origin of tissue impulse response **T**: scatterers

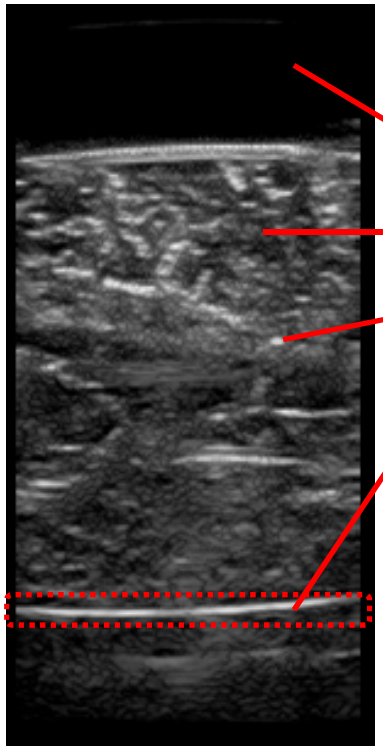

B-mode image of bovine liver sample in water

A useful classification method for scatterers:

[Szabo 2004, pp. 244-245; Greenleaf and Sehgal 1992]

Class 0: << λ molecules (absorption, e.g. water, protein)

Class 1: <λ scatterers (speckle, e.g. cells, e.cellular matrix)

Class 2: ~λ scatterers (distinguishable scatterer, e.g. bubble)

Class 3: >λ specular boundary (e.g. organ boundary)

Consider three scattering models:

1. discrete (point or with point origin) scatterer
2. inhomogeneous continuum
3. discrete-continuum hybrid

Point scatterer model

- Use p derived from FD method
- Projection of scatterers onto 2-D imaging plane
- Here, using point scatterers with same scattering strength
- As concentration of scatterers increases, packing constraints make scatterers more regular [Hete and Shung 1993]
- Instead of making location of scatterers totally random
  - have 10 μm × 10 μm pixels (typical cell size ~10 μm)
  - specify C_s: average number of scatterers per resolution cell
  - calculate probability of pixel containing a scatterer
  - sum contributions from each scatterer
- How does varying scatterer concentration C_s change scattering properties?
  - qualitative appearance of B-mode image
  - histogram of B-mode values
  - consider power spectrum of average of axial auto-correlations of beamformed image B

Point scatterer model: $C_s = 0.01$

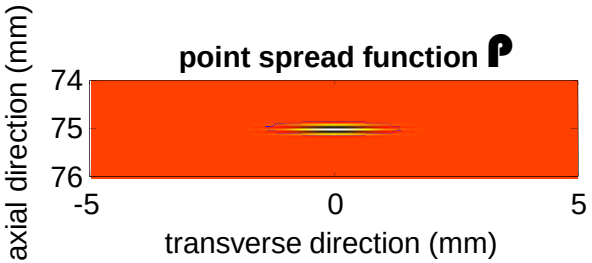

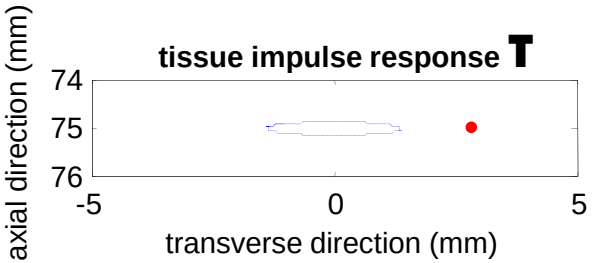

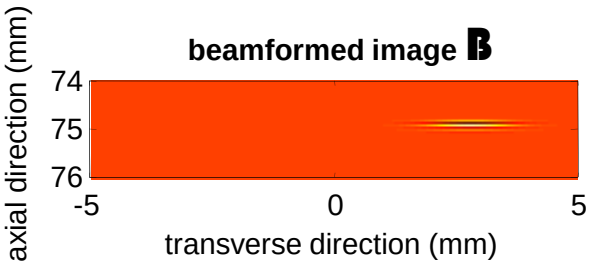

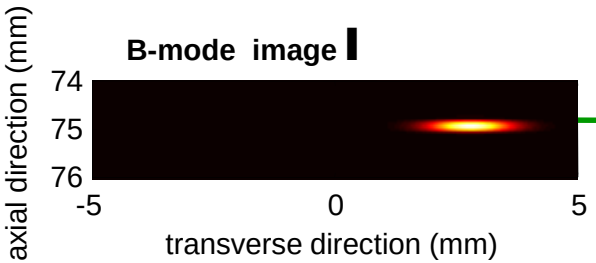

single scatterer does not have chance to interfere with other scatterers

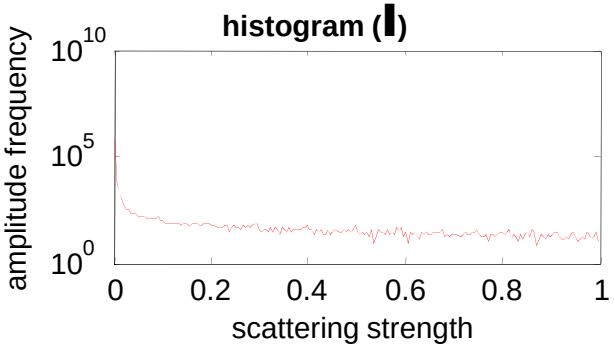

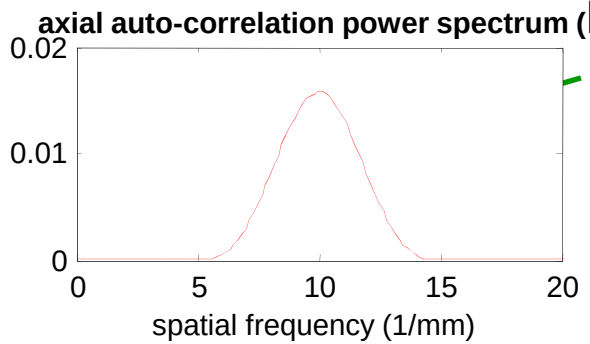

autocorrelation PSD is therefore simply square of power spectrum of pulse

Point scatterer model: $C_s = 0.1$

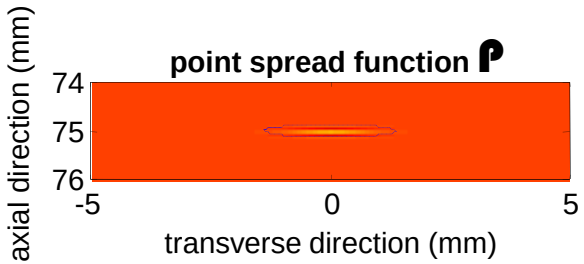

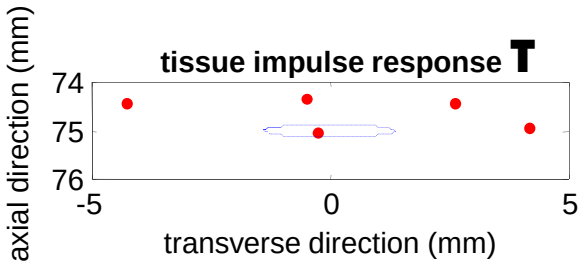

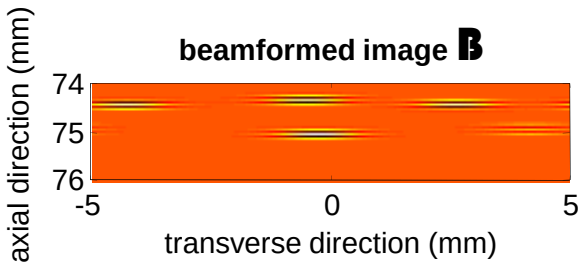

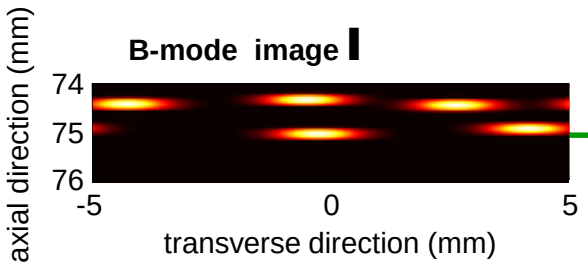

scatterers still far enough away that they can be distinguished from each otherx

as with previous histogram, most pixels have a values near 0, with 1 only at the scatterer locations

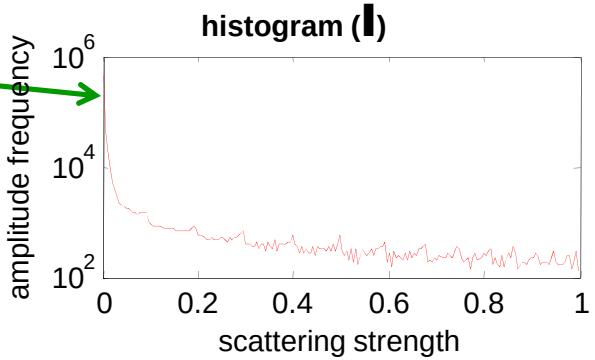

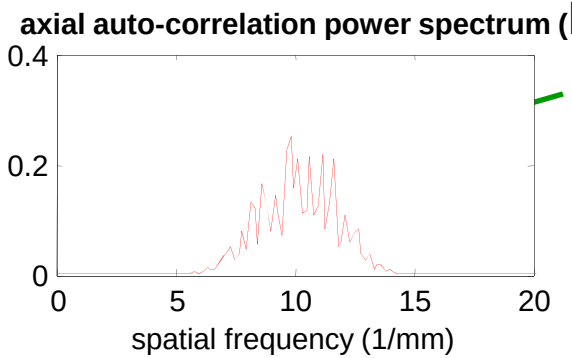

autocorrelation PSD however contains peaks from interference between scatterers

Point scatterer model: $C_s = 1$

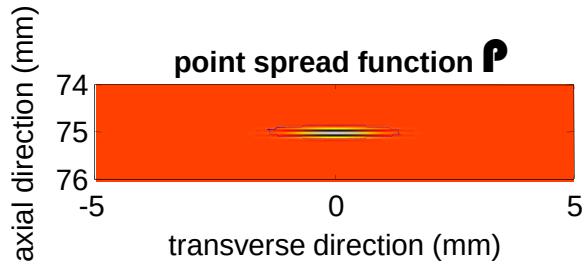

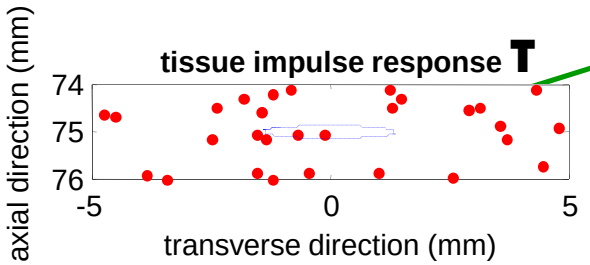

there are now often several scatterers inside one resolution cell

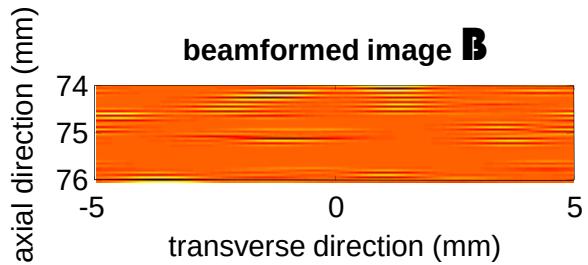

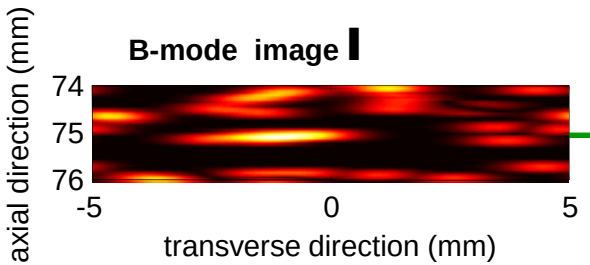

as a result, many scatterers are difficult to distinguish from each other

values above 1 are starting to appear due to constructive interference between scatterers

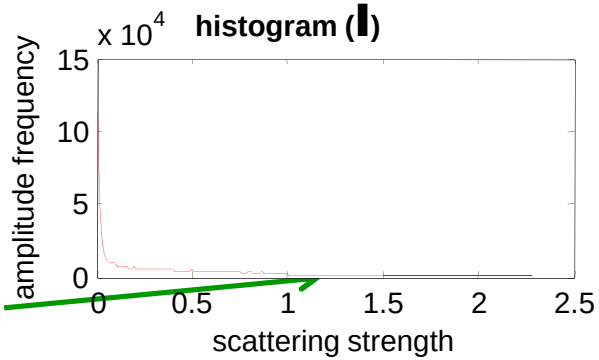

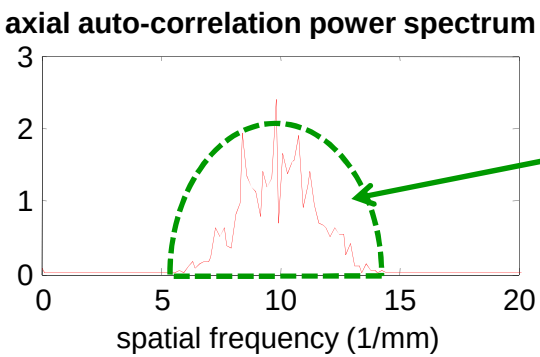

note that general distribution of power spectrum remains unchanged: that is, the fundamental speckle size due to the psf

Point scatterer model: $C_s = 10$

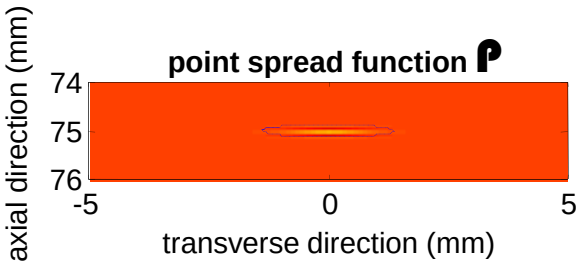

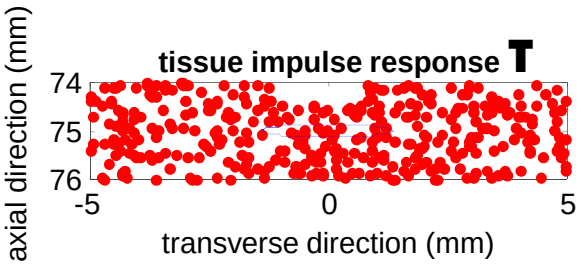

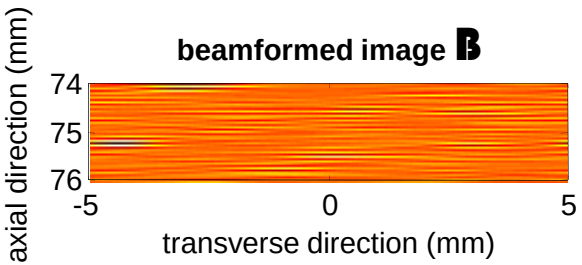

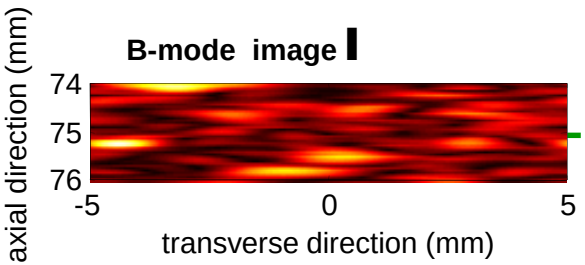

- scatterers at distances from each other that are comparable to distance between cycles of transmitted pulse
- **destructive** interference can now also occur as well as constructive
- at this point, effect of psf deviates from traditional “optic psf”

- marked change in histogram
- Rayleigh-like distribution
- resolution cell with average of 10 scatterers means that most values are no longer near 0

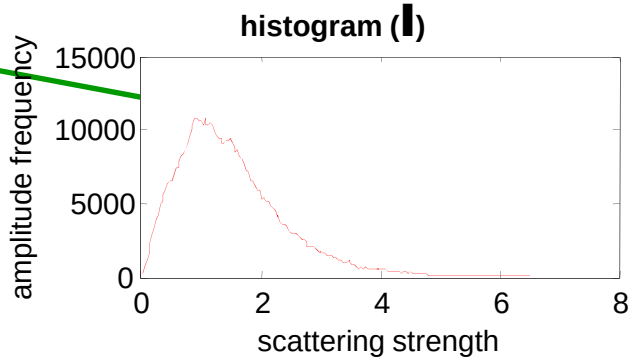

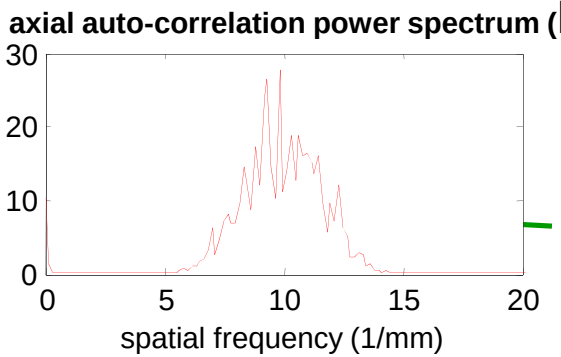

a DC component has appeared

Point scatterer model: $C_s = 100$

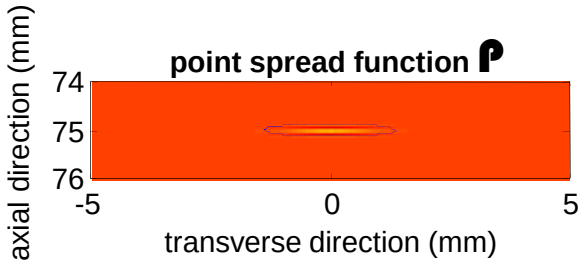

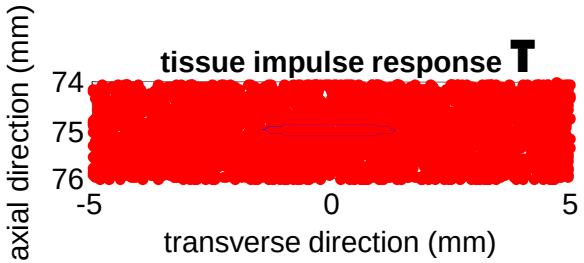

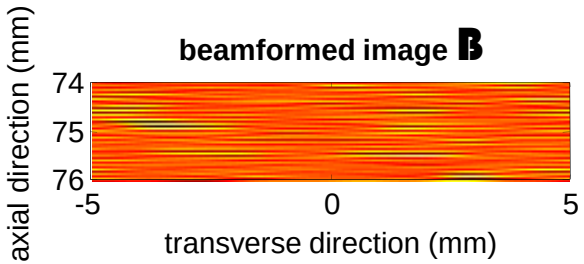

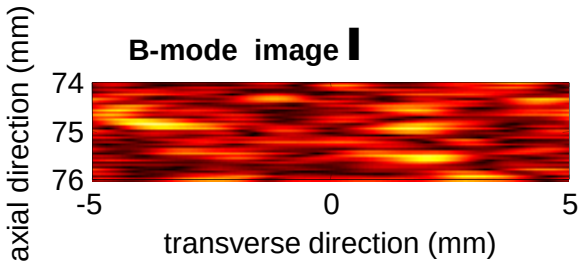

•distribution still Rayleigh-like
•increasing number of scatterers by 10 only caused modest increase in mean!

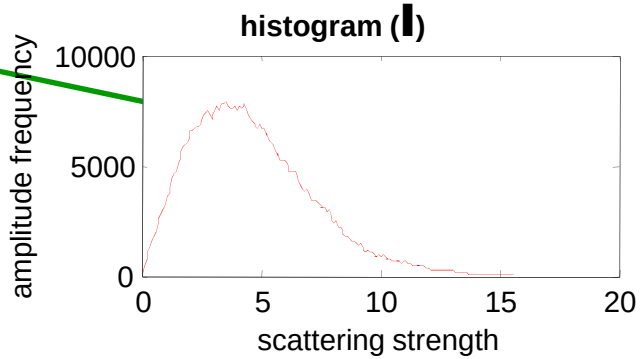

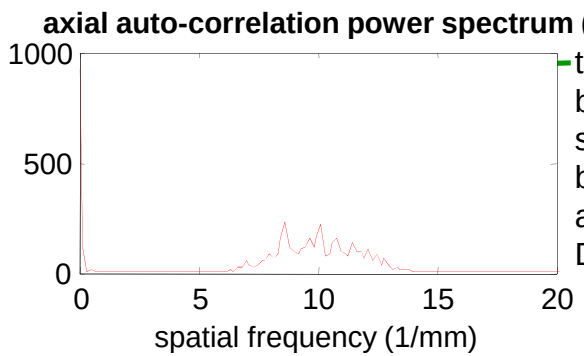

the scatterers are beginning to be significantly constrained by the 10μm×10μm grid, as evidenced by large DC component

Point scatterer model: $C_s = 1000$

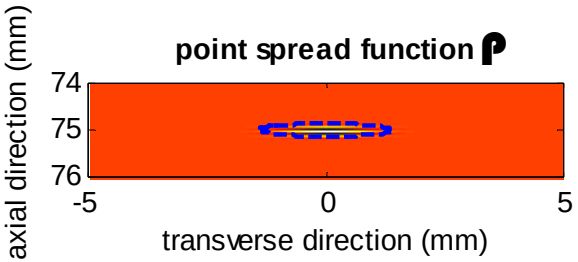

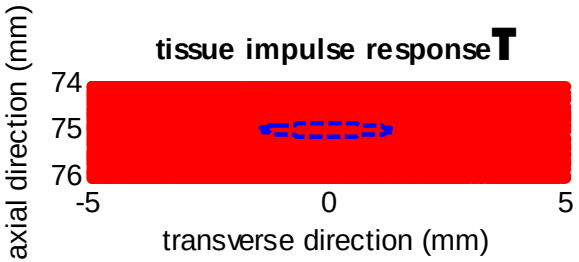

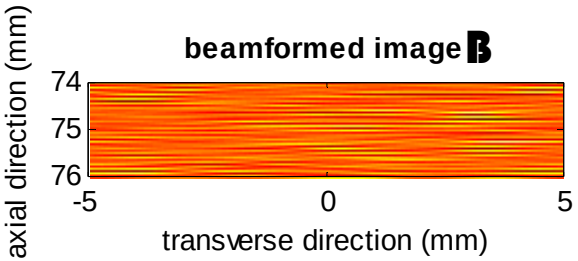

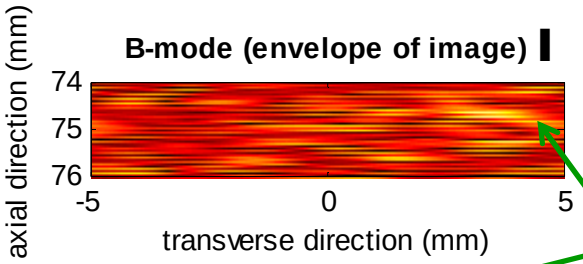

image dominated by DC term

addition of DC component creates Rician distribution

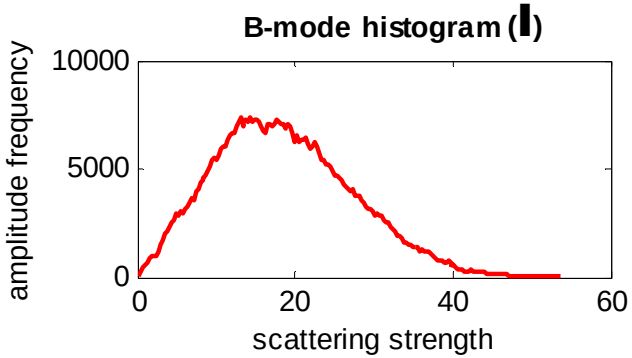

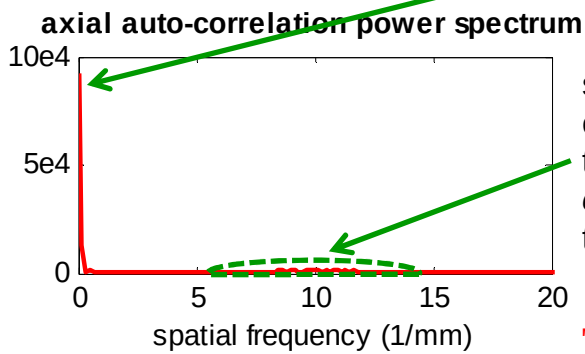

shape of non-DC component very similar to single-scatterer case: *cf* van Cittert-Zernike theorem

[Anderson and Trahey 2006]

Point scatterer model: explanation of observations

- Apart from DC term at high C_s, auto-correlation retains shape of **p**

C_s ~ 1 and lower

- Scatterers do not interfere: histogram of amplitudes reflects histogram of **p**

C_s ~ 10-100

- Phase of backscatter components independent of each other
- Total i (in-phase) and q (quadrature) components arise from addition of individual i_i and q_i components (assumed independent) from each scatterer s_i
- Central Limit Theorem: i and q have mean=0 Gaussian distributions
- Backscatter envelope $|\mathbf{I}| = (i^2+q^2)^{1/2}$ is therefore **Rayleigh-distributed**

C_s ~ 1000 and higher

- 10 μm × 10 μm pixel grid constraint: i_i, q_i no longer independent
- scattering has coherent component
- mean≠0 Gaussian i, q: $|\mathbf{I}|$ is Rician distributed [Anderson and Trahey 2006]

Inhomogeneous continuum model

- In limit of mean scatterer concentration $C_s \to \infty$, scattering strength=$1/C_s$
  - spatial distribution of scatterers becomes continuous
  - equivalent to inhomogeneous continuum model with small compressibility changes
  - (Note: density changes are usually neglected due to their angle-dependent scatter, although they can also be readily incorporated assuming backscatter – see earlier lecture, "Fundamental Concepts in Acoustics", slide title "Sub-wavelength scattering")
- Suppose medium completely characterised by spatial autocorrelation R_γ of its fractional changes in compressibility, $\gamma=(\kappa-\kappa_0)/\kappa$
- **B-mode spatial autocorrelation function** $R_\mathbf{I} = R_\gamma *_\mathbf{r} \rho$
- Random distribution of point or $<<\lambda$ particles ($R_\gamma \; \alpha \; \delta(\mathbf{r})$):

$$R_\mathbf{I} = \rho$$

[Anderson&Trahey 2006;Hill *et al.* 2004, p. 217;Mallart&Fink 1991;Wagner *et al.* 1983]

  - $R_\mathbf{I}$ only dependent on imaging system! (cf "Point scatterer model: C_s = 1000")
- Other R_γ tissue models: fluid sphere, spherical shell, Gauss [Insana *et al.* 1991]

Inhomogeneous continuum model:

its use in quantitative ultrasound (QUS)

- By choosing a tissue model for autocorrelation R_γ, one can predict the spatial autocorrelation of the image $R_\mathbf{I}$
- If $R_\mathbf{I}$ is taken along the imaging axis (A-lines), scaled $2/c$ to get the temporal autocorrelation and Fourier transformed, we obtain the frequency response of the scattering medium [Oelze *et al.* 2002], which is proportional to the oft-used term *form factor* (see [Insana *et al.* 1990] for definition)
- The chosen tissue model is parameterised by the scatterer diameter a_r (or, in the case of a Gaussian auto-correlation, effective diameter)
- By fitting the frequency response over a gated depth to the theoretical frequency response, the (effective) scatterer diameter may be estimated
- Example 1: slope of response using Gaussian model finds a_r, so identification of several slopes reveals scattering sources in kidney [Insana *et al.* 1991]
- Example 2: fit resonance peaks of spherical particles to Faran model to estimate size [Condliffe 2009]

Hybrid scattering model

[Mo and Cobbold 1992; Lim *et al.* 1996; Cobbold 2007, pp. 315-319]

- Consider voxels $<\lambda/10$ where phase is nearly constant throughout
- Scatterers in each voxel "add up" to create single equivalent scatterer
- Volume of equivalent scatterer equal to sum of volumes
- Centre of scatterer equal to centre of phase (for equivalent scatterers, this equals centre of mass [Lim *et al.* 1996])
- Computational gain over calculating scattering from individual scatterers

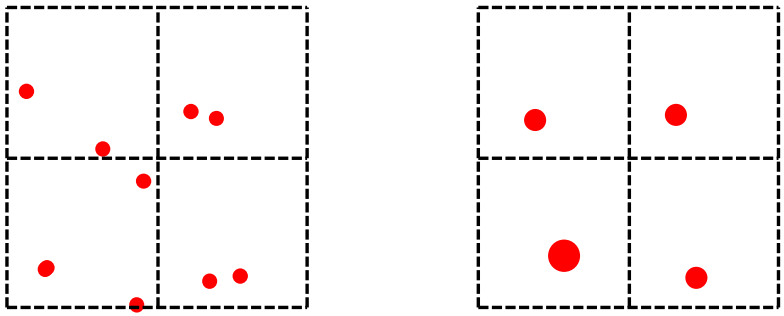

2-D representation of hybrid model. Left: original scatterers. Right: equivalent scatterers for each pixel. Adapted from [Lim *et al.* 1996].

Summary of lecture

- Considered methods to estimate point spread function p
- Considered several tissue models

How realistic are these models?

- Hexagonal close packing in liver [Doyle 2009] gives coherent speckle
- Some tissues agree well with continuum autocorr. models [Insana *et al.* 1991]
- Blood agrees well with hybrid model [Hill 2004, p. 213]

Effects we have neglected:

- Reflection (e.g. organ boundaries). Need anatomic info [Dillenseger et al. 2009]
- Attenuation. Simple to incorporate. TGC partially compensates for it.
- Instrumentation noise. More significant at larger depths due to attenuation
- Spatial invariance of p. SIR able to model it; dynamic apodization reduces it.
- Non-linear propagation of sound
- Multiple scattering

Ultrasound simulation packages

- Abersim http://www.ntnu.no/isb/abersim *non-linear acoustics!*
- Field II http://server.electro.dtu.dk/personal/jaj/field/)
- Ultrasim http://heim.ifi.uio.no/~ultrasim/
- Delfi http://www.mathworks.com/matlabcentral/fileexchange
- DREAM http://www.signal.uu.se/Toolbox/dream/

References

[Anderson and Trahey 2006] A seminar on *k*-space applied to medical ultrasound. http://dukemil.bme.duke.edu/Ultrasound/k-space/index.htm

[Cobbold 2007] Foundations of biomedical ultrasound

[Condliffe 2009] Particle characterization by acoustic microscopy following needle-free injection

[Dillenseger *et al.* 2009] Fast simulation of ultrasound images from a CT volume

[Doyle *et al.* 2009] Simulation of elastic wave scattering in cells and tissues at the microscopic level

[Ellis *et al.* 2007] A spline-based approach for computing spatial impulse responses

[Greenleaf and Sehgal 1992] Biologic system evaluation with ultrasound

[Gyöngy 2010] Passive cavitation mapping for monitoring ultrasound therapy

[Hete and Shung 1993] Scattering of ultrasound from skeletal muscle tissue

[Hill *et al.* 2004] Physical principles of medical ultrasonics

[Insana *et al.* 1990] Describing small-scale structure in random media using pulse-echo ultrasound

...

References

...

[Insana *et al* . 1991] Identifying acoustic scattering sources in normal renal parenchyma from the anisotropy in acoustic properties

[Jensen 1999] Linear description of ultrasound imaging systems. http://cmp.felk.cvut.cz/cmp/courses/ZSL2/cviceni/ultra12/ref_jaj_1999.pdf

[Lim *et al.* 1996] Particle and voxel approaches for simulating ultrasound backscattering from tissue

[Mallart and Fink 1991] The van Cittert--Zernike theorem in pulse echo measurements

[Mast 2007] Fresnel approximations for acoustic fields of rectangularly symmetric sources

[Mo and Cobbold 1992] A unified approach to modeling the backscattered Doppler ultrasound from blood

[Oelze *et al.* 2002] Ultrasonic characterization of tissue microstructure

[Olympus 2006] Ultrasonic transducers technical notes. http://www.olympus-ims.com/data/File/panametrics/UT-technotes.en.pdf

[Wagner *et al.* 1983] Statistics of speckle in ultrasound B-Scans